Analysis of two-dimensional non-equilibrium model of linear reactive chromatography considering irreversible and reversible reactions

Shamsul Qamar,[*,†,‡] Sadia Perveen,[‡] and Andreas Seidel-Morgenstern[†]

†*Max Planck Institute for Dynamics of Complex Technical Systems, Magdeburg, Germany*

‡**Department of Mathematics, COMSATS Institute of Information Technology, Islamabad, Pakistan*

E-mail: *qamar@mpi-magdeburg.mpg.de

Abstract

This article presents semi-analytical solutions and analytical temporal moments of a two-dimensional non-equilibrium transport model of linear reactive chromatography considering irreversible ($A \rightarrow B$) and reversible ($A \rightleftharpoons B$) reactions. The model is formed by a system of four coupled partial differential equations accounting for linear advection, longitudinal and radial dispersions, rate of variation of the local concentration of each component in the stationary phase, local deviation from equilibrium concentrations, and first order chemical reactions in both liquid and solid phases. The solution process successively employs Hankel transformation, Laplace transformation, and linear transformation steps to uncouple the governing set of coupled differential equations. The resulting uncoupled systems of ordinary differential equations are solved using an elementary solution technique. The numerical Laplace inversion is applied for back transformation of the solutions in the actual time domain. To analyze the effects of different kinetic parameters, statistical temporal moments are derived from the

Hankel and Laplace transformed solutions. The current solutions extend and generalize the recent solutions of a two-dimensional non-equilibrium single-solute transport model for non-reactive liquid chromatography. Analytical results are compared with the numerical solutions of a high resolution finite volume scheme for two sets of boundary conditions. Several case studies are carried. Good agreements in the results verify both the correctness of the analytical solutions and accuracy of the suggested numerical algorithm.

Introduction

The coupling of chemical reactions and chromatographic separation in a single unit leads to an integrated process known as reactive chromatography. Within a chromatographic reactor, the conversion of reactants and the separation of components take place simultaneously. The technique is useful to enhance conversion of the reactants and purity of the product. It adds significant improvements in the process performance and has, therefore, gained industrial popularity in the past few decades.[1–20]

In reactive chromatography rectangular pulses of reactants are periodically fed into the inert carrier stream. For instance, consider an irreversible reaction of the type A $\rightarrow$ B. In this case, rectangular pulses of reactant A are periodically fed into the carrier stream. During the transport of reactant A through the column, it reacts to form the product B. Different affinities of components A and B produce different migration velocities of the reactant and product, which leads to their separation. Complete conversion could be possible if the residence time of reactant A in the chromatographic reactor is long enough.

Mathematical modeling and simulation of chromatographic reactors have received considerable attention in the recent years. Such modeling approach was found useful for understanding the transport mechanisms, to scale up physio-chemical parameters, and to optimize the experimental conditions. Analytical solutions of these models are possible when equilibrium and mass transfer processes are represented by linear relationships.[1,21–26] An extensive dis-

cussion on such solutions is provided by Ruthven.[27] The derived analytical solutions could be useful to understand the effect of different kinetic parameters and to improve the process. Moment analysis is an effective technique for deducing important information about the retention equilibrium and mass transfer kinetics in a fixed-bed column or reactor. The moment generating property of the Laplace domain solutions can be utilized to obtain analytical moments. These moments can be used to get important information about the retention times, band broadenings, and front asymmetries. In the literature, several authors have derived and thoroughly discussed moments for various boundary conditions (BCs).[21,27–38] Further work on the moments analysis for fixed bed chromatographic systems using various boundary conditions can also be found in the literature.[27,35,39–45]

In this manuscript analytical solutions and temporal moments are derived for a two-dimensional non-equilibrium transport model of linear reactive chromatography considering irreversible ($A \rightarrow B$) and reversible ($A \rightleftharpoons B$) reactions. Liquid and solid phase reactions, rectangular pulse injections, and two sets of boundary conditions are considered. The current solutions extend and generalize the recent solutions of a two-dimensional single-solute non-equilibrium transport model for non-reactive liquid chromatography.[45] The analytical solutions of the model equations are derived through successive implementation of Hankel transformation, Laplace transformation, and eigen-decomposition technique. In the current scenario, no analytical Laplace inversion is possible. Therefore, numerical Laplace inversion is applied to get back semi-analytical solutions in the actual time domain.[46] To analyze the effects of different kinetic parameters, statistical temporal moments are derived from the Hankel and Laplace transformed solutions. A high resolution upwind finite-volume scheme (HR-FVS) is used to numerically approximate the model equations.[15,47] To illustrate the potential of the model, several case studies are carried out considering a wide range of mass transfer and reaction kinetics. The derived semi-analytical results are critically checked against the numerical solutions of suggested finite volume scheme.

The major novelty of this article specifically include: (a) derivation of analytical solutions

of linear two-dimensional lumped kinetic model (2D-LKM) of a chromatographic reactor for two different sets of boundary conditions, (b) consideration of both liquid and solid-phase reactions, (c) injection of specific profiles to amplify the effect of possible rate limitations of the mass transfer in the radial direction, (d) derivation of useful moment expressions, and (e) validation of the correctness of analytical results by the successful comparison with numerical results. The derived first three moments can be used to study the chromatographic behaviors, such as peak area, sample retention time, band broadening, asymmetry of elution profiles, and efficiency of the column. The derived analytical solutions are seen as helpful for further developments of chromatographic reactors. For instance, the analysis could be used to study the effects of mass transfer and reaction kinetics on the elution profiles, for sensitivity analysis, for validating numerical solutions, and for determining longitudinal and radial dispersion coefficients from experimentally determined elution profiles, among others. The studied 2D-model is more general and flexible than the classical 1D-models.[44] Moreover, we have provided useful solutions to apply this model, if required. The latter means if radial dispersion is rate limiting.

The remaining parts of the paper are organized as follows. In Section 2, the analytical solution of the model is derived for irreversible reaction. In Section 3, this analysis is extended to the study of reversible reactions. In Section 4, analytical temporal moments are derived from the Laplace transformed solutions for both irreversible and reversible reactions. Section 5 presents the results of various case studies. Finally, conclusions are drawn in Section 6.

Irreversible reaction (A→B)

This section considers the transport of a two-component solute in a two-dimensional chromatographic reactor of cylindrical geometry as depicted in Figure 1. In the current scenario, the component A (component 1) converts to B (component 2) through an irreversible first order reaction. The corresponding reaction rate constants of the liquid and solid phases are

denoted by $\tilde{\mu}_i$ and $\tilde{\nu}_i$ $(i = 1, 2)$, respectively. Let t denotes the time coordinate, z represents the axial coordinate along the column length and r is the radial coordinate along the column radius. The reactant and product travel along the column axis in the z-direction by advection and axial dispersion, spread along the column radius in the r-direction by radial dispersion, and reactant decays into produce product due to first order chemical reactions in liquid and solid phases. The considered two-component reactive lumped kinetic model (RLKM) incorporates the rate of variation of the local concentration of solutes in the stationary phase and a local deviation from equilibrium concentrations. The model lumps hereby the contribution of internal and external mass transport resistances into a mass transfer coefficient k_i for i-th component. It is further assumed that solute undergoes linear adsorption and chemical reactions are represented by first order kinetics. The following particular injection conditions are assumed to amplify the effects of mass transfer in the radial direction. The inlet cross section of the column is divided into an inner cylindrical core and an outer annular ring (see Figure 1) by introducing a new parameter $\bar{r}$. The injection can be done either through an inner core, an outer ring or through the whole cross section. The latter case results if $\bar{r}$ is set equal to the radius of the column denoted by R. Since in the latter case no initial radial gradients are provided, the solutions should converge into the solution of the simpler one-dimensional model.[44]

Based on the above setup, the mass balance equations of a two-dimensional RKLM considering irreversible reaction (A→B) can be expressed as

$$\frac{\partial c_1}{\partial t} + u\frac{\partial c_1}{\partial z} = D_z\frac{\partial^2 c_1}{\partial z^2} + D_r\left(\frac{\partial^2 c_1}{\partial r^2} + \frac{1}{r}\frac{\partial c_1}{\partial r}\right) - \frac{k_1}{\epsilon}(q_1^* - q_1) - \tilde{\mu}c_1\,, \tag{1}$$

$$\frac{\partial c_2}{\partial t} + u\frac{\partial c_2}{\partial z} = D_z\frac{\partial^2 c_2}{\partial z^2} + D_r\left(\frac{\partial^2 c_2}{\partial r^2} + \frac{1}{r}\frac{\partial c_2}{\partial r}\right) - \frac{k_2}{\epsilon}(q_2^* - q_2) + \tilde{\mu}c_1\,. \tag{2}$$

For solid phase, the mass balance equations are given as

$$\frac{\partial q_1}{\partial t} = \frac{k_1}{1-\epsilon}(q_1^* - q_1) - \tilde{\nu} q_1 \,, \tag{3}$$

$$\frac{\partial q_2}{\partial t} = \frac{k_2}{1-\epsilon}(q_2^* - q_2) + \tilde{\nu} q_1 \,. \tag{4}$$

In this study, equilibrium linear adsorption isotherms are considered, i.e.

$$q_i^* = a_i c_i, \qquad i = 1, 2 \,. \tag{5}$$

In the above equations, $c_i(t, r, z)$ denotes the liquid phase concentrations of the component i, $q_i(t, r, z)$ represents the non-equilibrium solid phase concentration, a_i denotes the linear adsorption isotherm (or Henry's coefficient), u is the interstitial velocity, D_z and D_r represent the longitudinal and radial dispersion coefficients, and $\epsilon \in (0, 1)$ is the external porosity. For sufficiently large value of k_i, the solution of RLKM converges to that of reactive equilibrium dispersive model (REDM).[21]

To simplify the analysis, the following dimensionless variables are introduced:

$$\begin{gathered} x = \frac{z}{L}, \quad \tau = \frac{ut}{L}, \quad \rho = \frac{r}{R}, \quad Pe_z = \frac{Lu}{D_z}, \quad Pe_r = \frac{R^2 u}{D_r L} \quad \kappa_i = \frac{k_i L}{u}, \\ \mu_i = \frac{\tilde{\mu}_i L}{u}, \quad C_i = \frac{c_i}{c_0} \quad Q_i = \frac{q_i}{c_0} \,, \quad \nu_i = \frac{\tilde{\nu}_i L}{u} \,, \quad c_0 = \max(c_{i,\mathrm{inj}}), \end{gathered} \tag{6}$$

where L is the length of the column, $c_{i,\mathrm{inj}}$ is the injected concentration of i-th component, and Pe_z and Pe_r are the dimensionless Peclet numbers in longitudinal and radial directions, respectively. Using these variables in Eqs. (1)-(5), we obtain

$$\frac{\partial C_1}{\partial \tau} = \frac{1}{Pe_z}\frac{\partial^2 C_1}{\partial x^2} - \frac{\partial C_1}{\partial x} + \frac{1}{Pe_r}\left(\frac{\partial^2 C_1}{\partial \rho^2} + \frac{1}{\rho}\frac{\partial C_1}{\partial \rho}\right) - \frac{\kappa_1}{\epsilon}(a_1 C_1 - Q_1) - \mu C_1 \,, \tag{7}$$

$$\frac{\partial C_2}{\partial \tau} = \frac{1}{Pe_z}\frac{\partial^2 C_2}{\partial x^2} - \frac{\partial C_2}{\partial x} + \frac{1}{Pe_r}\left(\frac{\partial^2 C_2}{\partial \rho^2} + \frac{1}{\rho}\frac{\partial C_2}{\partial \rho}\right) - \frac{\kappa_2}{\epsilon}(a_2 C_2 - Q_2) + \mu C_1 \,, \tag{8}$$

$$\frac{\partial Q_1}{\partial \tau} = \frac{\kappa_1}{(1-\epsilon)}(a_1 C_1 - Q_1) - \nu Q_1 \,, \tag{9}$$

$$\frac{\partial Q_2}{\partial \tau} = \frac{\kappa_2}{(1-\epsilon)}(a_2 C_2 - Q_2) + \nu Q_1 \,. \tag{10}$$

The initial condition in non-dimensionalized form are given as

$$C_i(\tau = 0, \rho, x) = C_{i,\text{init}} \,, \qquad 0 \le x \le 1 \,, \quad 0 < \rho \le 1 \,, \tag{11}$$

where $C_{i,\text{init}} = \frac{c_{i,\text{init}}}{c_0}$ is the dimensionless initial concentration of i-th component in the column. The corresponding radial boundary conditions (BCs) at $\rho = 0$ and $\rho = 1$, are expressed as

$$\frac{\partial C_i(\tau, \rho = 1, x)}{\partial \rho} = 0, \qquad \frac{\partial C_i(\tau, \rho = 0, x)}{\partial \rho} = 0 \,. \tag{12}$$

Moreover, two axial BCs are needed at the column inlet and outlet. In this study, two sets of axial BCs are considered which are summarized below.

Case 1. Dirichlet inlet BCs for concentration pulse of finite width:

At the column inlet, two types of injection are considered, such as injection in the inner cylindrical region or in the outer annular ring.

For inner cylindrical region injection, the Dirichlet BCs are expressed as

$$C_i(\tau, \rho, x = 0) = \begin{cases} C_{i,\text{inj}} \,, & \text{if } 0 \le \rho \le \bar{\rho} \quad \text{and} \quad 0 \le \tau \le \tau_{\text{inj}} \,. \\ 0 \,, & \bar{\rho} \le \rho \le 1 \quad \text{or} \quad \tau > \tau_{\text{inj}} \,, \end{cases} \tag{13}$$

while, for injection in the outer annular region, they are expressed as

$$C_i(\tau, \rho, x = 0) = \begin{cases} C_{i,\text{inj}} \,, & \text{if } \bar{\rho} \le \rho \le 1 \quad \text{and} \quad 0 \le \tau \le \tau_{\text{inj}} \,, \\ 0 \,, & 0 \le \rho \le \bar{\rho} \text{ or } \tau > \tau_{\text{inj}} \,. \end{cases} \tag{14}$$

Here, $C_{i,\mathrm{inj}} = \frac{c_{i,\mathrm{inj}}}{c_o}$ is the injected dimensionless concentration of i-th component, τ_{inj} is the dimensionless time of injection and

$$\bar{\rho} = \frac{\bar{r}}{\bar{R}}\,, \tag{15}$$

where $\bar{r}$ represents the radius of inner cylindrical core as shown in Figure 1. For injection over the whole inlet cross section, either $\bar{\rho} = 1$ in Eq. (13) or $\bar{\rho} = 0$ in Eq. (14) .

At the column outlet, the zero Neumann BCs for hypothetically infinite length column are given as

$$\frac{\partial C_i(\tau, \rho, x = \infty)}{\partial x} = 0\,. \tag{16}$$

Case 2. Danckwerts inlet BCs for concentration pulse of finite width:

In this case, the inlet BCs for inner zone injection are expressed as

$$C_i(\tau, \rho, x = 0) - \frac{1}{Pe_z}\frac{\partial C_i(\tau, \rho, x = 0)}{\partial x} = \begin{cases} C_{i,\mathrm{inj}}\,, & \text{if } 0 \le \rho \le \bar{\rho} \quad \text{and} \quad 0 \le \tau \le \tau_{\mathrm{inj}}\,, \\ 0\,, & \bar{\rho} \le \rho \le 1 \quad \text{or} \quad \tau > \tau_{\mathrm{inj}}\,, \end{cases} \tag{17}$$

while, for injection in the outer annular zone, we have

$$C_i(\tau, \rho, x = 0) - \frac{1}{Pe_z}\frac{\partial C_i(\tau, \rho, x = 0)}{\partial x} = \begin{cases} C_{i,\mathrm{inj}}\,, & \text{if } \bar{\rho} < \rho < 1 \quad \text{and} \quad 0 < \tau < \tau_{\mathrm{inj}}\,, \\ 0\,, & 0 \le \rho \le \bar{\rho} \quad \text{or} \quad \tau > \tau_{\mathrm{inj}}\,. \end{cases} \tag{18}$$

At the outlet of the column, the following Neumann BCs are used:

$$\frac{\partial C_i(\tau, \rho, x = 1)}{\partial x} = 0\,. \tag{19}$$

The analytical solutions of the above model for the considered two sets of BCs are presented in Appendix S1.

Reversible reaction $A \rightleftharpoons B$

Now, the more general case of linear reversible reactions is presented. In the case considered, component A (component 1) will be converted to component B (component 2) with reaction rate constants $\tilde{\mu}_1$ and $\tilde{\nu}_1$. Because of the reversibility of the reaction, component B is converted partly back to component A with reaction rate constants $\tilde{\mu}_2$ and $\tilde{\nu}_2$. The model equations for liquid phase are formulated as

$$\frac{\partial c_1}{\partial t} + u\frac{\partial c_1}{\partial z} = D_z\frac{\partial^2 c_1}{\partial z^2} + D_r\left(\frac{\partial^2 c_1}{\partial r^2} + \frac{1}{r}\frac{\partial c_1}{\partial r}\right) - \frac{k_1}{1-\epsilon}(q_1^* - q_1) - \tilde{\mu}_1 c_1 + \tilde{\mu}_2 c_2\,, \tag{20}$$

$$\frac{\partial c_2}{\partial t} + u\frac{\partial c_2}{\partial z} = D_z\frac{\partial^2 c_2}{\partial z^2} + D_r\left(\frac{\partial^2 c_2}{\partial r^2} + \frac{1}{r}\frac{\partial c_2}{\partial r}\right) - \frac{k_2}{1-\epsilon}(q_2^* - q_2) + \tilde{\mu}_1 c_1 - \tilde{\mu}_2 c_2\,. \tag{21}$$

For solid phase, the balance laws are expressed as

$$\frac{\partial q_1}{\partial t} = \frac{k_1}{1-\epsilon}(q_1^* - q_1) - \tilde{\nu}_1 q_1 + \tilde{\nu}_2 q_2\,, \tag{22}$$

$$\frac{\partial q_2}{\partial t} = \frac{k_2}{1-\epsilon}(q_2^* - q_2) + \tilde{\nu}_1 q_1 - \tilde{\nu}_2 q_2\,, \tag{23}$$

where q_1^* and q_2^* are given by Eq. (5). On using the dimensionless variables in Eq. (6), the above equations can be rewritten as

$$\frac{\partial C_1}{\partial \tau} + \frac{\partial C_1}{\partial x} = \frac{1}{Pe_z}\frac{\partial^2 C_1}{\partial x^2} + \frac{1}{Pe_r}\left(\frac{\partial^2 C_1}{\partial \rho^2} + \frac{1}{\rho}\frac{\partial C_1}{\partial \rho}\right) - \frac{\kappa_1}{\epsilon}(a_1 C_1 - Q_1) - \mu_1 C_1 + \mu_2 C_2\,, \tag{24}$$

$$\frac{\partial C_2}{\partial \tau} + \frac{\partial C_2}{\partial x} = \frac{1}{Pe_z}\frac{\partial^2 C_2}{\partial x^2} + \frac{1}{Pe_r}\left(\frac{\partial^2 C_2}{\partial \rho^2} + \frac{1}{\rho}\frac{\partial C_2}{\partial \rho}\right) - \frac{\kappa_2}{\epsilon}(a_2 C_2 - Q_2) + \mu_1 C_1 - \mu_2 C_2\,, \tag{25}$$

$$\frac{\partial Q_1}{\partial \tau} = \frac{\kappa_1}{(1-\epsilon)}\Big[a_1 C_1 - Q_1\Big] - \nu_1 Q_1 + \nu_2 Q_2\,, \tag{26}$$

$$\frac{\partial Q_2}{\partial \tau} = \frac{\kappa_2}{(1-\epsilon)}\Big[a_2 C_2 - Q_2\Big] + \nu_1 Q_1 - \nu_2 Q_2\,. \tag{27}$$

The same initial and boundary conditions are used as given by Eqs. (11)-(19).

The analytical solutions of this model for the considered two sets of BCs are given in Appendix S2.

Moment analysis

Moment analysis is a well-established method in chromatography that provides condensed information in the form of a relatively small number of temporal moments. It can be applied in various ways, namely (a) to describe in a simpler manner essential features of the chromatograms, (b) to estimate efficiently free model parameters by matching measured and predicted moments, (c) to efficiently predict performance parameters of the separations and, thus, (d) to optimize more easily the process.[21,27,31,32,34,41,43] In this study, we addressed essentially just the aspect (a). The zeroth moment describes the peak area (mass), the first moment corresponds to the retention time, the second central moment or variance provides significant information related to mass transfer processes in the column, while the third central moment analyzes the fronts asymmetries (skewness).

In the current 2D case, analytical moments for cylindrical pulses of finite width could be determined from the Laplace and Hankel transformed concentrations $\bar{C}_{iH}$ $(i = 1, 2)$ for both irreversible and reversible reactions cases. The general expression for the j-th moment of component i is given as

$$\mu_{jH}^{(i)} = (-1)^n \lim_{s \to 0} \frac{d^j(\bar{C}_{iH}(s, \lambda_n, x))}{ds^j}, \quad j = 0, 1, 2, \cdots . \tag{28}$$

The actual moments $\mu_j(\rho)$ are generated from Eq. (S1-6) by taking moments of the concentrations on both sides of that relation. On multiplying both sides of Eq. (S1-6) with τ^j and

integrating over τ from 0 to ∞, we obtain

$$\mu_j^{(i)}(\rho) = 2\mu_{jH}^{(i)}(\lambda_n = 0) + 2\sum_{n=1}^{\infty} \mu_{jH}^{(i)}(\lambda_n) \frac{J_0(\lambda_n \rho)}{|J_0(\lambda_n)|^2} \,. \tag{29}$$

From the above moments, the averaged non-normalized temporal moments $M_{i,\mathrm{av}}$ are obtained as

$$M_{j,\mathrm{av}}^{(i)} = 2\int_0^1 \mu_j^{(i)}(\rho)\rho d\rho \,, \quad j = 0, 1, 2, \cdots \,. \tag{30}$$

Finally, the normalized averaged temporal moments are available as[21]

$$\mu_{0,\mathrm{av}}^{(i)} = M_{0,\mathrm{av}}^{(i)}, \quad \mu_{j,\mathrm{av}}^{(i)} = \frac{M_{j,\mathrm{av}}^{(i)}}{\mu_{0,\mathrm{av}}^{(i)}}, \quad j = 1, 2, 3, \cdots \,. \tag{31}$$

The averaged time dependent cental moments $\mu'_{n,av}$ $(n = 2, 3)$ are evaluated as

$$\mu'^{(i)}_{2,\mathrm{av}} = \mu_{2,\mathrm{av}}^{(i)} - (\mu_{1,\mathrm{av}}^{(i)})^2 \,, \tag{32}$$

$$\mu'^{(i)}_{3,\mathrm{av}} = \mu_{3,\mathrm{av}}^{(i)} - 3\mu_{1,\mathrm{av}}^{(i)}\mu_{2,\mathrm{av}}^{(i)} + 2(\mu_{1,\mathrm{av}}^{(i)})^3 \,. \tag{33}$$

The corresponding j-th central moments of the band profile at the outlet of a column of length $x = 1$ are numerically obtained using the expression

$$\mu'^{(i)}_{j,\mathrm{av}} = \frac{\int_0^\infty C_{i,\mathrm{av}}(x = 1, \tau)\,(\tau - \mu_1)^j d\tau}{\mu_{0,\mathrm{av}}^{(i)}} \,, \quad j = 2, 3, \tag{34}$$

where

$$C_{\mathrm{i,av}}(x, \tau) = 2\int_0^1 C_i(\rho, x, \tau)\rho d\rho \,. \tag{35}$$

Complete derivations of moments, using availability of solutions in the Hankel-Laplace do-

mains and the moment generating property of this transformation for both boundary conditions, are presented in the Appendix S3 considering regenerated system, i.e. $C_{i,\text{init}} = 0$ for $i = 1, 2$.

The above moments are presented in terms of the dimensionless time coordinate τ. However, they can be easily expressed in term of the actual time coordinate $t = L\tau/u$ as follows:

$$\mu_{0H}^{(i)}(t) = \frac{L}{u}\mu_{0H}^{(i)}(\tau), \qquad \mu_{jH}^{(i)}(t) = \left(\frac{L}{u}\right)^{j} \mu_{jH}^{(i)}(\tau), \;\; j = 1, 2, \cdots . \tag{36}$$

The above formulas were used in the test problems to plot averaged moments with dimensions.

In the discussion of test problems, a comparison and analysis of analytically and numerically determined temporal moments are presented. The numerical moments were obtained by integrating the profiles obtained from the HR-FVS.[47] Eqs. (34) and (35) were used to integrate the concentration profiles of semi-analytical solutions or HR-FVS to get the numerical moments. The trapezoidal rule is applied to numerically approximate the integral terms appearing in these equations.

Numerical test problems

The derived analytical solutions of the previous sections were analyzed by considering several test problems. For validation, the derived analytical solutions were compared with the numerical results of HR-FVS.[47,48] The basic parameters use to illustrate the behavior of a chromatographic reactor are listed in Table 1.

Problem 1: Linear irreversible reaction

In this first series of illustrating test problems, semi-analytical solutions obtained through numerical Laplace inversion and HR-FVS are compared for the irreversible reaction. The

results obtained show the effects of both liquid and solid phase reactions, types of boundary conditions used, and mass transfer coefficients.

In Figure 2 the concentration profiles are plotted at the column outlet by taking injection through inner cylindrical zone in an empty column ($C_{i,\text{init}} = 0$ for $i = 1, 2$) using Dirichlet BCs. Both components are injected to the column (i.e. $C_{1,\text{inj}} = 1.0\,,\, C_{2,\text{inj}} = 0.5\,$). In Figures 2a and 2b solid phase reaction is neglected ($\nu = 0$). Where as in Figures 2c and 2d both liquid and solid phase reactions are considered. In both cases, component 1 with larger adsorption equilibrium constant elutes later from the column as compared to the component 2 having smaller value of the adsorption equilibrium constant. The amount of product (component 2) increases when reaction is considered both in both liquid and solid phases. Good agreements can be observed in the concentration profiles of semi analytical solutions and HR-FVS.

Figure 3 provides a comparison of analytical and numerical solutions for injections through the outer zone with Danckwerts BCs for less axial back mixing $Pe_z = 600$ and slower radial transport $Pe_r = 15$. Both semi-analytical solutions and numerical results of HR-FVS are compared. For both liquid and solid phase reactions the amount of product increases and reactant decreases faster than the case when liquid phase reaction is considered only. Good agreement was found in the results of numerical Laplace inversion and HR-FVS.

Figure 4a demonstrates the effect of reaction rate constant μ in the liquid phase, while keeping the solid phase reaction rate constant ν fixed. On the other hand, Figure 4b illustrates the effect of reaction rate constant in the solid phase, while keeping the liquid phase reaction rate μ fixed. In both cases $C_{i,\text{init}} = 0.0$ for $i = 1, 2$, $C_{1,\text{inj}} = 1.0$ and $C_{2,\text{inj}} = 0.0\,$. Once again, the amount of reactant decreases and product increases on increasing the influence of reaction rate constants.

Figure 5a analyzes the effects of BCs for two different values of Pe_z considering $C_{1,\text{inj}} = 1.0\,$, $C_{2,\text{inj}} = 0.5$, $C_{i,\text{init}} = 0.0$ for $i = 1, 2$, $Pe_r = 15$, $\mu = 1.067$, and $\nu = 0.027$. Clear differences are evident between the profiles obtained by using Dirichlet and Danckwerts BCs for relatively large axial dispersion or small Peclet number. However, both Dirichlet and

Danckwerts BCs produce the same results for relatively high Peclet number. Figure 5b reveals the effects of mass transfer coefficients on the concentration profiles using Dankwert BCs and inner zone injection for $C_{i,\text{init}} = 0.0$ $(i = 1, 2)$, $C_{1,\text{inj}} = 1$ and $C_{2,\text{inj}} = 0.0$. Here, only liquid phase reaction is taken into account. The current solution profiles are broadened for small values of κ_i and are converging to the solution of EDM for large values of κ_i.

Figure 6 displays the first three local moments $\mu_i(\rho)$ $(i = 1, 2, 3)$ for component 1 (Figures 6a, 6b and 6c) and component 2 (Figures 6d, 6e and 6f), plotted along the radial coordinate of the column for fixed $D_z = 0.01\, cm/min^2$, $u = 1.5\, cm/min$ and the varying $Pe_{ratio} = \frac{R^2 D_z}{L^2 D_r}$. In these plots of moments only reactant is injected to the column ($C_{1,\text{inj}} = 1$ and $C_{2,\text{inj}} = 0$) and solid phase reaction is neglected. The effect of radial dispersion coefficient is visible from the plots of first, second and third moments. For large value of radial dispersion coefficient or small Pe_{ratio}, these moments approach to constant values which is a limiting one-dimensional case.

In Figure 7 analytical and numerical average moments $\mu^{(i)}_{j,\text{av}}$ are presented as a functions of inverse flow rates using $C_{i,\text{init}} = 0$ for $i = 1, 2$, $\mu = 1.067$, $\nu = 0$, $C_{1,\text{inj}} = 1$, and $C_{2,\text{inj}} = 0$. The plots of zeroth moments show that conversion of component 1 into component 2 reduces on increasing the velocity. The plots of first moments depict that the retention time reduces on increasing the velocity and component 1 is more retained as compared to component 2. The second average central moments correspond to the variance of the elution profile. The variance of both components reduces on increasing the velocity. Moreover, the second average moment of components 1 and 2 intersect at $u = 18\, cm/min$, which indicates that for this particular flow rate both components have the same variance (spreading). The third averaged central moments corresponds to the asymmetry of the concentration profiles. The positive values of averaged central moments indicate that both profiles are right tailed. The plots of these moments for Dankwert BCs have similar behavior and are therefore omitted. It was also observed that moments for both inner and outer zone injections have similar behavior. Another time, good agreements can be observed between analytically and

numerically determined moments.

Problem 2: Linear reversible reaction

This second illustrating part focuses on the comparison of analytical and numerical results of two-component RLKM model for reversible reactions. Again, all parameters listed in Table 1 were used.

Figure 8 displays the comparison of analytical and numerical solutions using Dirichlet BCs with inner zone injection. In Figures 8a and 8b, only component 1 is injected (i.e. $C_{1,\text{inj}} = 1.0$ and $C_{2,\text{inj}} = 0$), where as in Figures 8c and 8d, both components are injected (i.e. $C_{1,\text{inj}} = 1.0$ and $C_{2,\text{inj}} = 0.5$). Moreover, reactions in both liquid and solid phases are taken into account ($\mu_1 = 1.067, \mu_2 = 0.533, \nu_1 = 0.027, \nu_2 = 0.013$). Because of reversibility of the reaction, the concentration levels are different for both components compared to the irreversible case shown in Figure 2. Now more amount of component 1 is unconverted and less amount of component 2 is produced.

Figure 9 depicts the comparison of analytical and numerical solutions using Dirichlet BCs with outer zone injection. Again in Figures 9a and 9b, only reactant is injected (i.e. $C_{1,\text{inj}} = 1$ and $C_{2,\text{inj}} = 0$), and reactions in both liquid and solid phases are taken into account, i.e. $\mu_1 = 1.067$, $\mu_2 = 0.533$, $\nu_1 = 0.027$ and $\nu_2 = 0.013$. While, in Figures 9c and 9d injections of both components are considered (i.e. $C_{1,\text{inj}} = 1$ and $C_{2,\text{inj}} = 0.5$). Again the reversibility of reaction is visible as concentration levels are different for both components compared to irreversible reaction shown in Figure 3.

In Figure 10, the plots of second and third central moments are presented as a functions of dimensionless mass transfer coefficient κ_i. In these plots, we considered $C_{1,\text{inj}} = 1$ and $C_{2,\text{inj}} = 0$, $\mu_1 = 1.067$, $\mu_2 = 0.533$ and solid phase reaction is neglected. Significant changes can be observed in the plots of second and third average central moment on varying κ_i from 1 to 50. However, this effect is negligible for $\kappa_i > 50$ and the results of 2D LKM converge to those of 2D EDM. Once again, both inner and outer zone injections revealed similar results.

With the solutions derived more instructive parametric calculations can be performed.

Conclusion

Accurate and quantitative information about the dynamics in a chromatographic reactor could be very useful for the appropriate design of the system and packing material. This article was focused on the analysis of 2D non-equilibrium models of linear reactive chromatography describing first order irreversible and reversible reactions. General analytical solutions were derived through successive implementation of the finite Hankel and Laplace transforms assuming rectangular pulse injections of finite widths, an initially pre-equilibrated column, and two sets of boundary conditions. Semi-analytical solutions in the actual time domain were derived through numerical Laplace inversion. Analytical temporal moments were derived from the Hankel-Laplace domain solutions. For validation, the semi-analytical results were compared with the numerical solutions of HR-FVS. The derived analytical solutions and moments could be useful for further developments of 2D chromatographic reactors. For instance, the analysis could be used to study in detail the effects of mass transfer and reaction kinetics on the elution profiles, for sensitivity analysis, and for validation of results obtained from newly introduced numerical schemes. The moment solutions could be effectively used for parameters estimation.

The considered 2D-model can be valuable in various situations, e.g. (a) the injection at the column inlet is not perfect (i.e. a radial profile is introduced at the column inlet), (b) the column is not homogeneously packed (which is more probable for larger columns), and (c) there are radial temperature gradients which are connected also with radial concentration gradients. All these issues occur in reality. Often they might be minor and even negligible, then justifying the 1D-model. However, for their relevance and effects 2D-models are required. With our isothermal model, we could just study situation (a) by assuming injections in the inner cylinder or outer annular region. Situations (b) and (c) are more complicated

and require further model extensions (considering non-constant column porosities and an energy balance), which are currently under investigation.

Supporting Information

Appendix S1: Analytical solutions for irreversible reaction.

Appendix S2: Analytical solutions for reversible reaction.

Appendix S3: Analytical moments.

This information is available free of charge via the Internet at http: //pubs.acs.org.

References

(1) Carta, G. Simultaneous Reaction and Chromatography. In *Chromatographic and Membrane Processes in Biotechnology*; Costa, C. A., Cabral J. S., Eds.; Kluwer Academic Publishers: The Netherlands, 1991, p429.

(2) Schweich, D.; Villermaux, J. The Chromatographic Reactor. A New Theoretical Approach. *Ind. Eng. Chem. Fundamen.* **1978**, *17*, 1.

(3) Cho, B. K.; Aris, R.; Carr, R. W. The Mathematical Theory of a Countercurrent Catalytic Reactor. *Proc. R. Soc. Lond. A* **1982**, *383*, 147.

(4) Petroulas, T.; Aris, R.; Carr, R. W. Analysis of the Counter-Current Moving-Bed Chromatographic Reactor. *Comput. Maths. Appl.* **1985**, *11*, 5.

(5) Takeuchi, K.; Uraguchi, Y. Separation Conditions of the Reactant and the Product with a Chromatographic Moving Bed Reactor. *J. Chem. Eng. Jpn.* **1976**, *9*, 164.

(6) Takeuchi, K.; Uraguchi, Y. Basic Design of Chromatographic Moving Bed Reactors for Product Refining. *J. Chem. Eng. Jpn.* **1976**, *9*, 246.

(7) Takeuchi, K.; Uraguchi, Y. The Effect of the Exhausting Section on the Performance of a Chromatographic Moving Bed Reactor. *J. Chem. Eng. Jpn.* **1977**, *10*, 72.

(8) Takeuchi, K.; Uraguchi, Y. Experimental Studies of a Chromatographic Moving-Bed Reactor-Catalytic Oxidation of Carbon Monoxide on Activated Alumina as a Model Reactor. *J. Chem. Eng. Jpn.* **1977**, *10*, 455.

(9) Takeuchi, K.; Miyauchi, T.; Uraguchi, Y. Computational Studies of a Chromatographic Moving Bed Reactor for Consecutive and Reversible Reactions. *J. Chem. Eng. Jpn.* **1978**, *11*, 216.

(10) Binous, H.; McCoy, B. J. Chromatographic Reactions of the Three Components: Application to Separations. *Chem. Eng. Sci.* **1992**, *47*, 4333.

(11) Ganetsos, G.; Barker, P.E. *Preparative and Production Scale Chromatography*; Marcel Dekker, Inc.: New York, 1993; Vol. 61, p 375.

(12) Borren, T.; Fricke, J.; Schmidt-Traub, H. (Eds.). *Chromatographic Reactors in Preparative Chromatography of Fine Chemicals and Pharmaceutical Agents*; Wiley-VCH Verlag: Weinheim, 2005, p 371.

(13) Fricke, J.; Schmidt-Traub, H.; Kawase, M. *Chromatographic Reactor, Ullmann's Encyclopedia of Industrial Chemistry*; Wiley-VCH Verlag: Weinheim, 2005.

(14) Javeed, S.; Qamar, S.; Seidel-Morgenstern, A.; Warnecke, G. A Discontinuous Galerkin Method to Solve Chromatographic Models. *J. Chromatogr. A* **2011**, *1218*, 7137.

(15) Javeed, S.; Qamar, S.; Seidel-Morgenstern, A.; Warnecke, G. Parametric Study of Thermal Effects in Reactive Liquid Chromatography. *Chem. Eng. J.* **2012**, *191*, 426.

(16) Qamar, S.; Bibi, S.; Khan, F.U.; Shah, M.; Javeed, s.; Seidel-Morgenstern, A. Irreversible and Reversible Reactions in a Liquid Chromatographic Column: Analytical Solutions and Moment Analysis. *Ind. eng. Chem. Res.* **2014**, *53*, 2461.

(17) Lin, B.; Song, F.; Guiochon, G. A nalytical Solution of the Ideal, Nonlinear Model of Reaction Chromatography for a Reaction A← B and a Parabolic Isotherm. *J. Chromatogr. A* **2003**, *1003*, 91.

(18) Yamaoka, K.; Nakagawa, T. Moment Analysis for Reaction Chromatography. *J. Chromatogr. A* **1976**, *117*, 1.

(19) Sardin, M.; Schweich, D; Villermaux, J.; Ganetsos, G.; Barker, P.E. (Eds.). *Preparative Fixed-Bed Chromatographic Reactor, Preparative and Production Scale Chromatography*; Marcel Dekker Inc.: New York, USA, 1993, p 477.

(20) Villermaux, J.; Rodrigues, A.E.; Tondeur, D. (Eds.). *The Chromatographic Reactor in Percolation Processes: Theory and application*; Sijthoffen Noordhoff; Alpena an den Rijn: The Netherlands, 1981, p 539.

(21) Guiochon, G.; Felinger, A.; Shirazi, D.G., Katti, A.M. *Fundamentals of Preparative and Nonlinear Chromatography*, 2nd ed; ELsevier Academic press: New York, 2006.

(22) Javeed, S.; Qamar, S.; Ashraf, W.; Seidel-Morgenstern, A.; Warnecke, G. Analysis and Numerical Investigation of Two Dynamic Models for Liquid Chromatography. *Chem. Eng. Sci.* **2013**, *90*, 17.

(23) Li, P.; Xiu, G.; Rodrigues, A.E. Analytical Solutions for Breakthrough Curves in a Fixed Bed of Shell-Core Adsorbent. *AIChE J.* **2003**, *49*, 2974.

(24) Li, P.; Xiu, G.; Rodrigues, A.E. Modeling Breakthrough and Elution Curves in a Fixed Bed of Shell-Core Adsorbent for Separation of Proteins-Exact Enalytical Solution and Approximate Solutions. *Chem. Eng. Sci.* **2003**, *59*, 3091.

(25) Li, P.; Yu, J.; Xiu, G.; Rodrigues, A.E. Perturbation Chromatography with Inert Core Adsorbent: Moment Solution for Two-Component Nonlinear Adsorption Isotherm. *Chem. Eng. Sci.* **2011**, *66*, 4555.

(26) Qamar, S.; Abbasi, J.N; Javeed, S.; Shah, M.; Khan, F.U.; Seidel-Morgenstern, A. Analytical Solutions and Moment Analysis of Chromatographic Models for Rectangular Pulse Injections, *J. Chromatogr. A* **2013**, *1315*, 92.

(27) Ruthven, D.M. *Principles of Adsorption and Adsorption Processes*; Wiley-Interscience: New York, 1984.

(28) Kubin, M. Beitrag zur Theorie der Chromatographie. *Collection of Czechoslovak Chemical Communications* **1965**, *30*, 1104.

(29) Kubin, M. Beitrag zur Theorie der Chromatographie II. Einfluss der Diffusion Ausserhalb und der Adsorption Innerhalb des Sorbens-Korns. *Collection of Czechoslovak Chem. Commun.* **1965**, *30*, 2900.

(30) Kucera, E. Contribution to the Theory of Chromatography: Linear Non-Equilibrium Elution Chromatography. *J. Chromatogr. A* **1965**, *19*, 237.

(31) Miyabe, K.; Guiochon, G. Influence of the Modification Conditions of Alkyl Bonded Ligands on the Characteristics of Reversed-Phase Liquid Chromatography. *J. Chromatogr. A* **2000**, 903, 1.

(32) Miyabe, K.; Guiochon, G. Measurement of the Parameters of the Mass Transfer Kinetics in High Performance Liquid Chromatography. *J. Separat. Sci.* **2003**, *26*, 155.

(33) Miyabe, K. Surface Diffusion in Reversed-Phase Liquid Chromatography Using Silica Gel Stationary Phases of Different C1 and C18 Ligand Densities. *J. Chromatogr. A* **2007**, *1167*, 161.

(34) Miyabe, K. Moment Analysis of Chromatographic Behavior in Reversed-Phase Liquid Chromatography. *J. Separat. Sci.* **2009**, *32*, 757.

(35) Schneider, P., Smith, J.M. Adsorption Rate Constants From Chromatography. *AIChE J.* **1968**, *14*, 762.

(36) Suzuki, M. Notes on Determining the Moments of the Impulse Response of the Basic Transformed Equations. *J. Chem. Eng. Jpn* **1973**, *6*, 540.

(37) Wolff, H.-J.; Radeke, K.-H; Gelbin, D. Heat and Mass Transfer in Packed Beds-IV: Use of weighted Moments to Determine Axial Dispersion Coefficient. *Chem. Eng. Sci.* **1980**, *34*, 101.

(38) Wolff, H.-J.; Radeke, K.-H; Gelbin, D. Weighted Moments and the Pore-Diffusion Model. *Chem. Eng. Sci.* **1980**, *35*, 1481.

(39) Mehta, R.V.; Merson, R.L.; McCoy, B.J. Hermite Polynomial Representation of Chromatography Elution Curves. *J. Chromatogr. A* **1974**, *88*, 1.

(40) Linek, F.; Duduković, M.P. Representation of Breakthrough Curves for Fixed-Bed Adsorbers and Reactors Using Moments of the Impulse Response. *Chem. Eng. J.* **1982**, *23*, 31.

(41) Javeed, S.; Qamar, S.; Ashraf, W.; Warnecke, G.; Seidel-Morgenstern, A. Analysis and Numerical Investigation of Two Dynamic Models for Liquid Chromatography. *Chem. Eng. Sci.* **2013**, *90*, 17.

(42) Qamar, S.; Abbasi, J.N.; Javeed, S.; Shah, M.; Khan, F.U.; Seidel-Morgenstern. Analytical Solutions and Moment Analysis of Chromatographic Models for Rectangular Pulse Injections. *J. Chromatogr. A* **2013**,*1315*, 92.

(43) Suzuki, M.; Smith, J.M. Kinetic Studies by Chromatography. *Chem. Eng. Sci.* **1971**, *26*, 221.

(44) Bibi, S.; Qamar, S.; Seidel-Morgenstern, A. Irreversible and Reversible Reactive Chromatography: Analytical Solutions and Moment Analysis for Rectangular Pulse Injections. *J. Chromatogr. A* **2015**, *1385*, 49.

(45) Parveen, S.; Qamar, S.; Seidel-Morgenstern, A. Two-Dimensional Non-Equilibrium Model of Liquid Chromatography: Analytical Solutions and Moment Analysis, *Chem. Eng. Sci.* **2015**, *122*, 64.

(46) Rice, R.G.; Do, D.D. *Applied Mathematics and Modeling for Chemical Engineers*; Wiley-Interscience: New York, 1995.

(47) Javeed, S.; Qamar, S.; Seidel-Morgenstern, A.; Warnecke, G. Efficient and Accurate Numerical Simulation of Nonlinear Chromatographic Processes. *J. Comput. Chem. Eng.* **2011**, *35*, 2294.

(48) Koren, B. *A Robust Upwind Discretization Method for Advection, Diffusion and Source Terms. In C. B. Vreugdenhil, B. Koren, editors, Numerical Methods for Advection-Diffusion Problems, Volume 45 of Notes on Numerical Fluid Mechanics*; Vieweg Verlag: Braunschweig, 1993, Chapter 5, p 117.

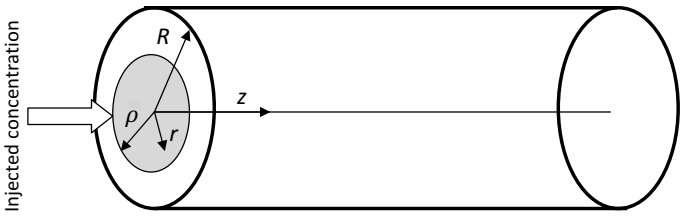

Figure 1: Schematic diagram of a chromatographic column of cylindrical geometry.

Table 1: Parameters used in the considered test problems of two-component RLKM.

Parameters	values
Length of the Column	$L = 4\ cm$
Radius of the Column	$R = 0.2\ cm$
Radius of inner zone	$\bar{r} = 0.1414\ cm$
Porosity	$\epsilon = 0.4$
Interstitial velocity	$u = 1.5\ cm/min$
Axial dispersion coefficient	$D_z = 0.01\ cm^2/min,\ Pe_z = 600$
Radial dispersion coefficient	$D_{\mathrm{r}} = 0.001\ cm^2/min,\ Pe_r = 15$
Injection time	$t_{\mathrm{inj}} = 1\ min$
Initial concentration of the i-th component	$C_{\mathrm{init}} = 0$
Adsorption equilibrium constant for component 1	$a_1 = 4.0$
Adsorption equilibrium constant for component 2	$a_2 = 1.0$
Mass transfer coefficient for component 1	$\kappa_1 = 2.67$
Mass transfer coefficient for component 2	$\kappa_2 = 2.67$
Irreversible liquid phase reaction rate constant	$\mu = 1.067$
Reversible liquid phase reaction rate constant (component 1)	$\mu_1 = 1.067$
Reversible liquid phase reaction rate constant (component 2)	$\mu_2 = 0.533$
Irreversible solid phase reaction rate constant	$\nu = 0.027$
Reversible solid phase reaction rate constant (component 1)	$\nu_1 = 0.027$
Reversible solid phase reaction rate constant (component 2)	$\nu_2 = 0.013$

Note that: $Pe_{\mathrm{ratio}} = \frac{R^2}{L^2}\frac{D_z}{D_r} = Pe_r/Pe_z = 0.025$ for $\frac{D_z}{D_r} = 10$.

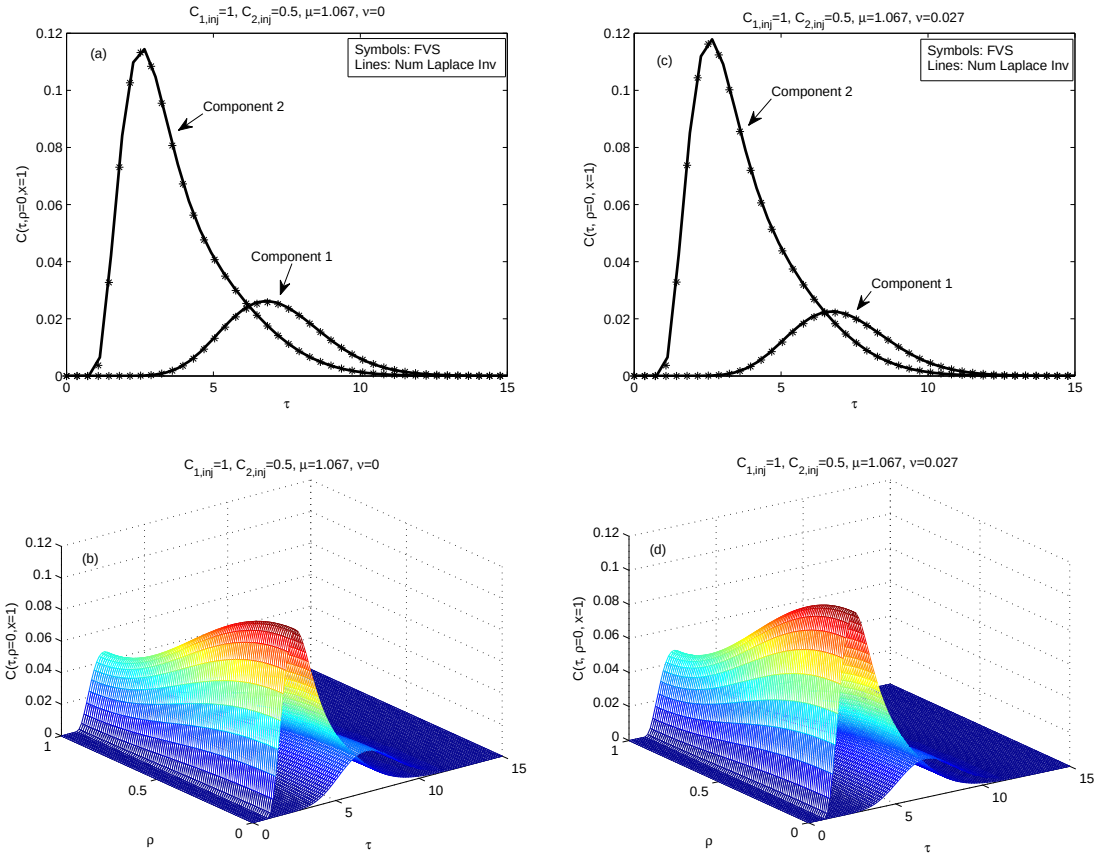

Figure 2: Irreversible reaction, plots (a) and (b): reaction in liquid phase only, plots (c) and (d): reaction in both liquid and solid phases. Sample is injected through inner zone using Dirichlet BCs and $C_{i,\text{init}} = 0$ for $i = 1, 2$, $Pe_r = 15$ and $Pe_z = 600$.

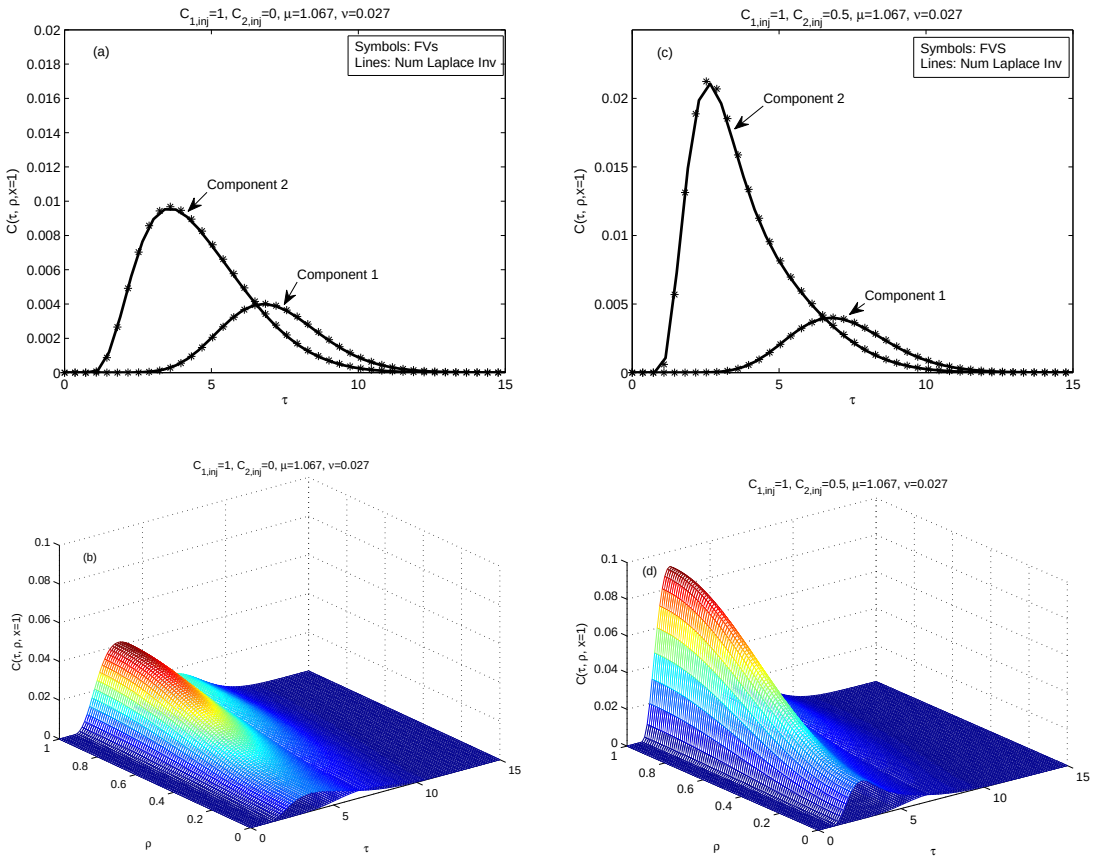

Figure 3: Irreversible reaction, plots (a) and (b): reaction in liquid phase only, plots (c) and (d): reaction in both liquid and solid phases. Sample is injected through outer zone using Danckwerts BCs and $C_{i,\text{init}} = 0$ for $i = 1, 2$, $Pe_r = 15$ and $Pe_z = 600$.

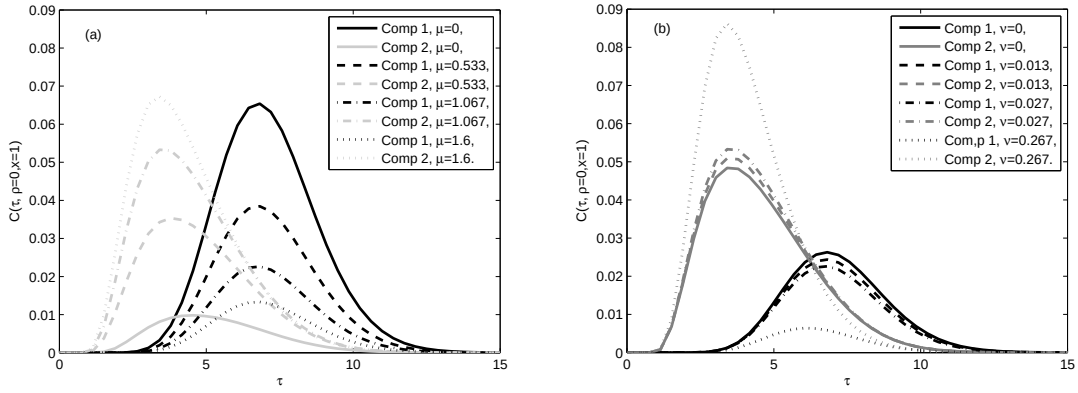

Figure 4: Irreversible reaction and injection through inner zone of radius $\bar{\rho}$ with Dirichlet BCs. (a) Comparison of solutions for different values of liquid phase reaction rate constant, (b) comparison of solution for different values of solid phase reaction rate constant.

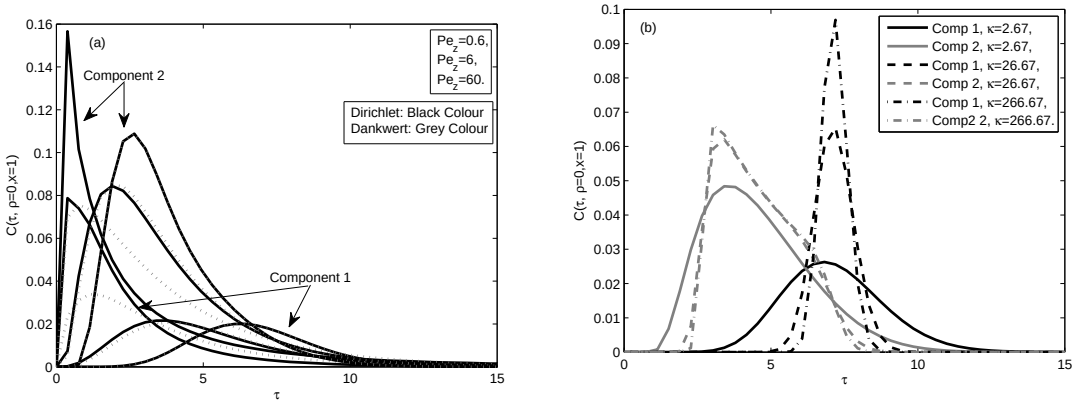

Figure 5: Irreversible reaction and injection through inner zone of radius $\bar{\rho}$. (a) Effects of BCs for different Pe_z with $C_{1,\text{inj}} = 1$, $C_{2,\text{inj}} = 0$, $C_{i,\text{init}} = 0$ for $i = 1, 2$ and fix $Pe_r = 15$. (b) effect of mass transfer coefficient on the solution profile using injection through inner zone using Danckwerts BCs.

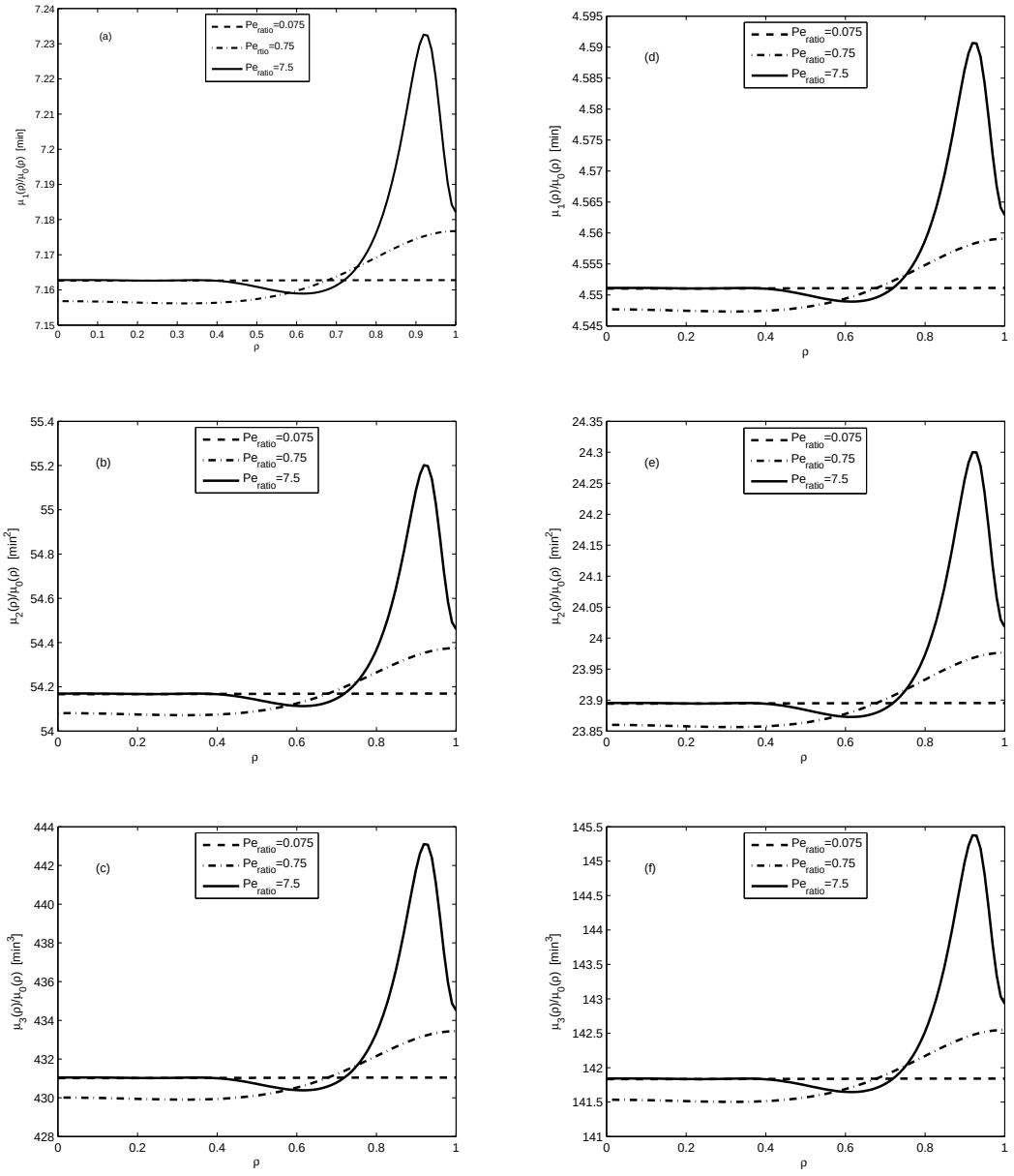

Figure 6: Dimensionless radial moments of irreversible reaction for inner zone injection. Effect of D_r on the local moments $\mu_i(\rho)$ for fixed $D_z = 0.01\,cm^2/min$ ($Pe_z = 600$). Varied is the ratio $Pe_{\text{ratio}} = \frac{R^2}{L^2}\frac{D_z}{D_r}$. Component 1: plots (a), (b) and (c), component 2: plots (d), (e) and (f).

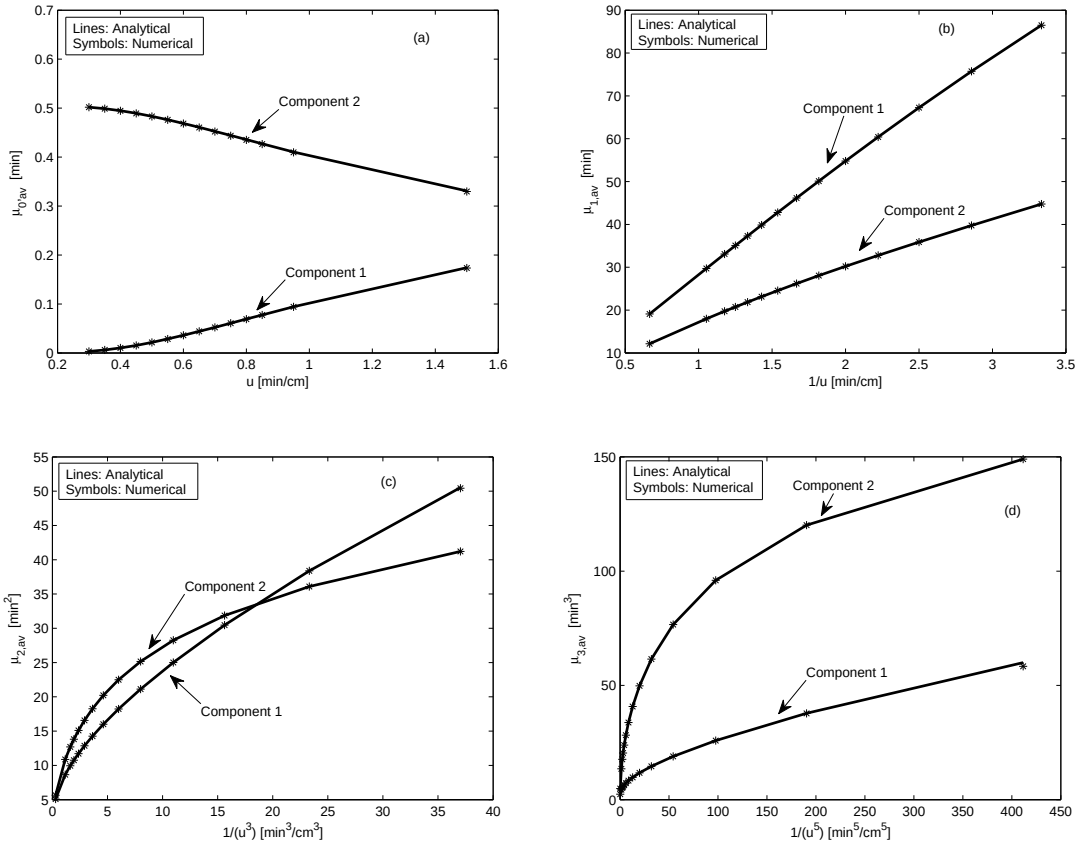

Figure 7: Injection through inner zone using Dirichlet BCs and $C_{i,\text{init}} = 0$ for $i = 1, 2$. Comparison of analytical and numerical averaged central moments with dimensions (c.f. Eq. (36)) considering different flow rates.

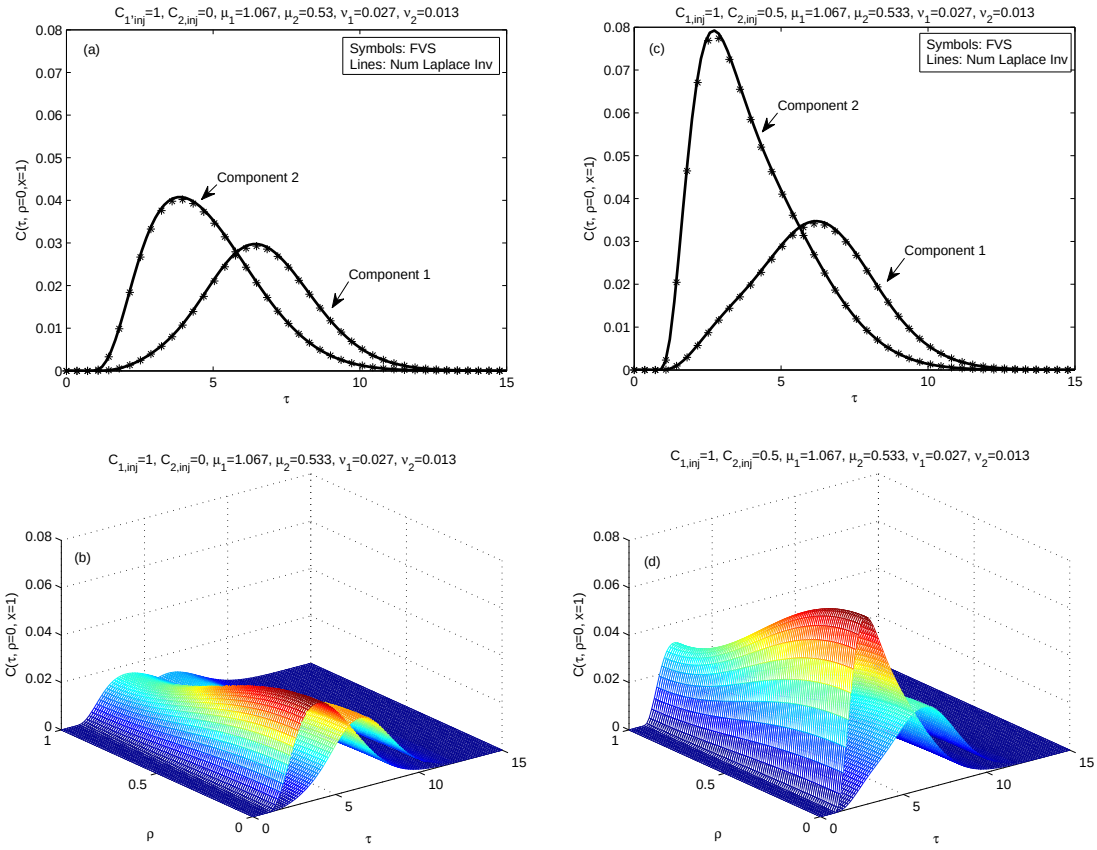

Figure 8: Reversible reaction: (a) reaction in liquid only, (b) reaction in both liquid and solid phase. Sample is Injected through inner zone with Dirichlet BCs and $C_{i,\text{init}} = 0$ for $i = 1, 2$, $Pe_r = 15$ and $Pe_z = 600$

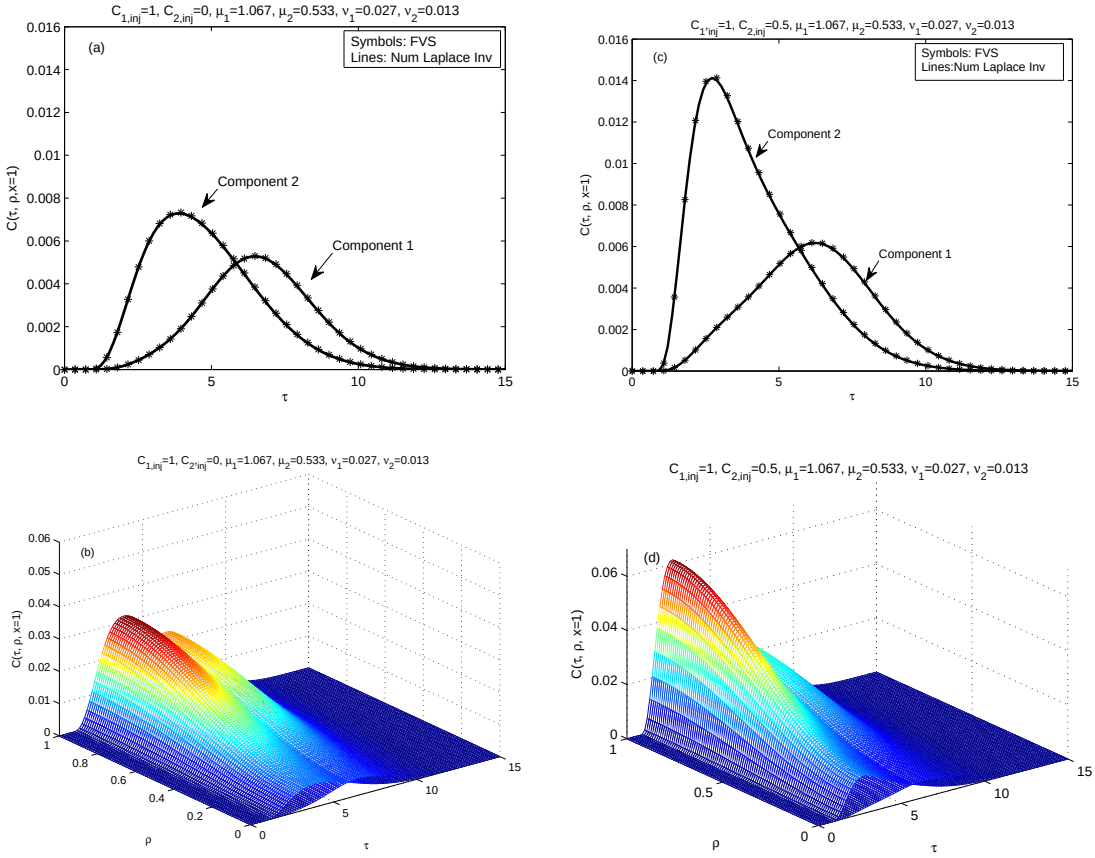

Figure 9: Reversible reaction: (a) reaction in liquid only, (b) reaction in both liquid and solid phase. Sample is Injected through outer zone with Dankwert BCs and $C_{i,\text{init}} = 0$ for $i = 1, 2$, $Pe_r = 15$ and $Pe_z = 600$

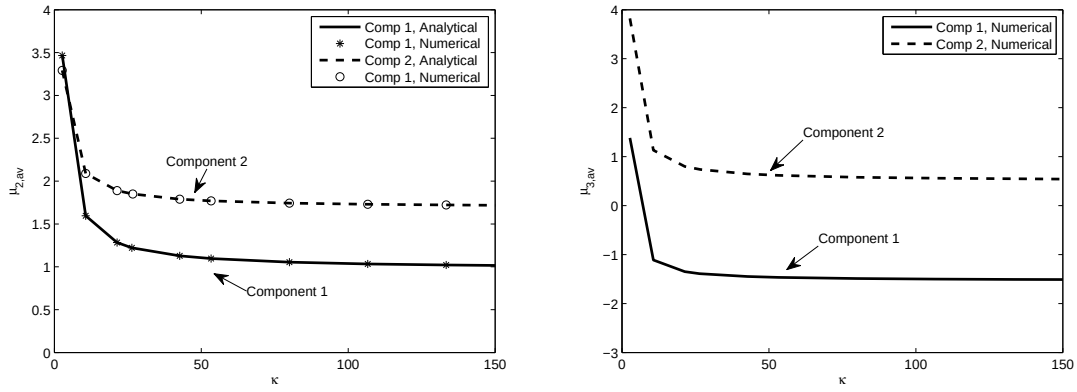

Figure 10: Reversible reaction: Effect of κ on dimensionless averaged moments for inner zone injection using $C_{i,\text{init}} = 0$ for $i = 1, 2$, $Pe_r = 15$, and $Pe_z = 600$.

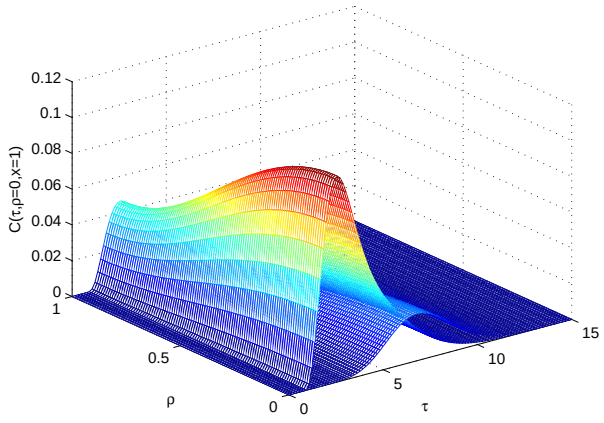

For Table of Contents only.